Journal of Structural Geology, Vol. 12, No. 8, pp. 995 to 1004, 1990
Printed in Great Britain

0191-8141/90 $03.00+0.00

Local variations in quartz [*c*]-axis orientations in non-coaxial regimes and their significance for the mechanics of *S–C* fabrics

A. KROHE

Institut für Geologie, Ruhr-Universität Bochum, D-4630 Bochum, Universitätsstrasse 150, F.R.G.

(*Received* 20 *April* 1989; *accepted in revised form* 8 *March* 1990)

Abstract—The quartz [*c*]-axis orientations of quartz-bearing *S–C* mylonites vary on the mm scale. Two specimens from different tectonic settings (the Variscan Schwarzwald, West Germany, and the Eastern Alps, Austria) are investigated. In the first specimen prism glide along ⟨*a*⟩ predominates, and in the second specimen basal glide along ⟨*a*⟩ predominates. In both specimens the pattern of [*c*]-axis variations is similar—it is suggested to be characteristic of *S–C* mylonites. On the local scale, there are two patterns of preferred orientation: (1) a crossed-girdle, 'type I', which is inclined in a sense opposite to the inferred overall sense of shear. This occurs in moderately strained domains; (2) a single-girdle, which is slightly inclined in the same sense as the inferred overall sense of shear. This occurs in domains that suffered higher strain. Both types are considered to reflect stable orientations of the 'easy glide direction; (crystallographic ⟨*a*⟩ direction), at different stages of the deformational history. Two kinematic interpretations are discussed. Quartz [*c*]-axis fabric variations reflect a spatial (and possibly also temporal) partitioning in flow path between domains that underwent either: (1) spinning coaxial flow and non-spinning non-coaxial flow; or (2) spinning non-coaxial flow and non-spinning non-coaxial flow, associated with variations in parameters of the deformation (such as magnitude of strain and strain rate) and perhaps also rate of recrystallization and recovery. In either interpretation, in moderately strained domains oblique [*c*]-axis girdles are generated that cannot be used as shear-sense indicators.

INTRODUCTION

DEFORMATION experiments on single crystals of quartz have revealed a considerable number of glide systems (e.g. Baëta & Ashbee 1969a,b, Hobbs *et al.* 1972, 1976, Ardell *et al.* 1974, Morrison-Smith *et al.* 1976, Twiss 1976, Kirby 1977, review in table I in Linker *et al.* 1984). However, in naturally deformed rocks the number of activated glide systems is limited, and most patterns of quartz [*c*]-axis preferred orientations develop by slip along the crystallographic ⟨*a*⟩ direction (Schmid & Casey 1986). The pattern of quartz [*c*]-axis preferred orientations mainly reflects the flow path (Law *et al.* 1984, 1986, Law 1986, 1987, Platt & Behrmann 1986, review by Price 1985). During coaxial deformation the ⟨*a*⟩ axes tend to align along preferred orientations which are symmetric to the principal directions of finite strain. The resulting [*c*]-axis girdles, which are oriented normal to the ⟨*a*⟩-axis maxima, are also disposed symmetrically about the principal directions of finite strain (Bouchez 1978). During non-coaxial deformation one ⟨*a*⟩ axis tends to align with the bulk shear direction; the resulting [*c*]-axis girdles are oriented normal to the bulk shear direction but oblique to the principal directions of finite strain. The sense of obliquity is directed towards the sense of shear (Eisbacher 1970, Bouchez 1978, Burg & Laurent 1978, Lister & Williams 1979, Van Roermund *et al.* 1979, Simpson 1980, Behrmann & Platt 1982, Simpson & Schmid 1983, Mancktelow 1985, 1987).

High homogeneous non-coaxial strain in large volumes of rock generates uniform quartz [*c*]-axis orientations that reflect the kinematics of the regional deformation (e.g. the 'Plattengneis' in the Austroalpine zone of the Alps, Krohe 1987). On the other hand, local variations in sense of vorticity and in magnitude, orientation and type of finite strain generate variations in quartz [*c*]-axis patterns on a very small scale. [*c*]-axis girdles, which locally are inclined in a direction opposite to the overall sense of vorticity, have been reported from quartz ribbons that flow around rigid feldspar porphyroclasts (Garcia Celma 1982), but they occur also in less obviously perturbed zones of pure quartz rocks (e.g. Passchier 1983).

In this article two quartz bearing *S–C* mylonites are investigated that exhibit variations in sense of asymmetry of quartz [*c*]-axis girdles on the mm scale. The specimens originate from different tectonic settings. The domainal variation in [*c*]-axis orientation is similar in both—it is suggested to be characteristic of *S–C* mylonites.

Specimen SW267 is a muscovite–cordierite-bearing metagranite from the southern Schwarzwald (the 'Badenweiler-Lenzkirch zone', West Germany). It was transformed to a mylonite during the early Carboniferous in a ductile thrust zone (Krohe & Eisbacher 1988). In the metasedimentary host rocks of the granite, syntectonic temperatures between 500 and 650°C are indicated by the synkinematically stable paragenesis sillimanite–muscovite–quartz. Cordierite retrogressed to white mica during and after the deformation. Intracrystalline slip, predominantly along the prism ⟨*a*⟩ system, is inferred from the quartz [*c*]-axis orientations (see Discussion).

Specimen KG3 is a garnet-bearing quartzite from the Austroalpine crystalline rocks ('Graden shear zone', east Austria). It was transformed to a mylonite during

the late Cretaceous, in a shear zone with extensional geometry (Krohe 1987). Syntectonic temperatures below 500°C are indicated by synkinematic retrogression of staurolite to white mica and chlorite in the presence of quartz. Intracrystalline slip, predominantly along the basal ⟨*a*⟩ system, is inferred from the quartz [*c*]-axis orientations (see Discussion).

MICROSTRUCTURAL ELEMENTS

Within the scale of a thin section, both specimens exhibit similar planar and linear fabrics. These are outlined diagrammatically in Fig. 1(a). A mesoscopic foliation is defined by a compositional layering made up of mineral aggregates of greater and lesser competence. It follows approximately the regional attitude of the shear zone and is considered to be nearly parallel to the direction of the overall shear plane. Two domains (A and B) that extend parallel to the mesoscopic foliation can be established which differ in magnitude of strain, deformation mechanisms and other parameters of the deformation (see also Vauchez 1987). Both domains are characterized by internal planar fabrics, defined by preferred orientation of the shapes of mineral aggregates (A- and B-foliations). The A-domains are moderately strained: the orientation of the internal A-foliation is considered to approximate the *XY* plane of a moderate finite strain in a non-coaxial flow field. The B-domains are highly strained: the orientation of the internal B-foliation (and lineation) is considered to approximate the *XY* plane (and *X*-direction) of a high finite strain in a non-coaxial flow field; it is nearly parallel to the mesoscopic foliation. The internal foliation of the A-domains makes an angle of about 30° to the internal foliation of the B-domains. Towards higher strain, the A-foliation grades into the B-foliation: quartz aggregates aligned parallel to A-foliation are bent towards the B-foliation (Figs. 1b & c). The A- and B-foliations also define external reference frames for the quartz [*c*]-axis pole figures. The contact between A- and B-domains are planar discontinuities that extend parallel to the mesoscopic foliation. Sometimes a small angle (about 3–5°) between discontinuity planes and the A-foliation favors the development of scarps on the mesocopic foliation plane. A fourth foliation is defined by the preferred orientation of elongate newly formed quartz grains, whose long axes are inclined in the sense of shear with respect to the mesocopic foliation (Fig. 2b). This foliation is considered to reflect the *XY* plane of the last strain increment after the formation of the new grain (Lister & Snoke 1984, Burg *et al.* 1986). The configuration of the A-foliation and the B-foliation/mesoscopic foliation may correspond to 'type I *S–C* fabrics' of Lister & Snoke (1984), and that of the quartz long-axis orientation and the B-foliation/mesoscopic foliation to 'type II *S–C* fabrics' of these authors. The youngest structures in both specimens are secondary sets of *C'*-planes (Platt & Vissers 1980).

MICROSTRUCTURES AND QUARTZ [*c*]-AXIS ORIENTATIONS

The microstructures suggest deformation in the A- and B-domains occurred after the thermal peak of metamorphism, but prior to cooling below 500°C (SW267) and 300°C (KG3). The deformation may be diachronous (see discussion below). However, the difference in age of deformation between the A- and B-domains is supposed to be small because rapid cooling is suggested for both Variscan and Austroalpine basements (Krohe 1987, Krohe & Eisbacher 1988). Both domains of specimens SW267 and KG3 (Fig. 1) are characterized by dynamic recrystallization of quartz, mica and (in SW267) feldspar.

Variations in magnitude of strain between the A- and B-domains reflect variations in flow strength between stronger and weaker phases or between structurally more or less weakened domains of the same phase. Quartz is present in both A- and B-domains. In both domains the quartz aggregates are made up of old grains deformed by crystal-plastic mechanisms and new grains formed by syntectonic recrystallization. In specimen KG3 the old grains show deformation lamellae inclined to the basal plane at about 25° (B-domains) and 35° (A-domains, Fig. 2d), undulatory extinction, deformation bands, and subgrains along deformation band boundaries and at grain boundaries. The development of new grains is associated with rotation of subgrains, Rotation recrystallization was followed by grain boundary migration. In specimen SW267 relict old grains are less frequent. In the *XY* section of both specimens, in the A- and B-domains newly formed grains are elongate and show a shape preferred orientation (Fig. 2b).

Adjacent quartz layers in the A- and B-domains of both specimens show closely spaced variations in: magnitude of strain (axial ratios of 3–4:1 in the A-domains and 10–30:1 in the B-domains), in grain-size distribution of new grains (Fig. 2a) and in quartz [*c*]-axis orientations (Figs. 1a–d). In the A-domains a relatively wide range of grain sizes (Fig. 2a) is the result of grain boundary migration (GBM) associated with grain growth. Local post-kinematic grain growth is indicated by irregular grain boundaries. In the B-domains newly formed grains exhibit a more uniform and generally smaller grain size, compared to the A-domains (around 35 μm, Fig. 2b).

Quartz [*c*]-axis measurements were carried out on sections cut perpendicular to the mesoscopic foliation and parallel to the lineation using a Universal stage. On the scale of the measurements quartz aggregates are more or less monomineralic. The ratio of grain boundaries/phase boundaries is >9 (Fig. 2c). A higher proportion of phase boundaries (17%) in the A-domain of specimen KG3 results from a thin mica layer within the quartz aggregate (see the sketch in Fig. 2).

In the A-domains of both specimens the quartz [*c*]-axis fabrics are 'type I' crossed-girdles in the sense of Lister (1977), with the fabric skeleton inclined at about 35–40° in a sense opposite to the overall sense of shear with respect to the mesoscopic foliation, and approxi-

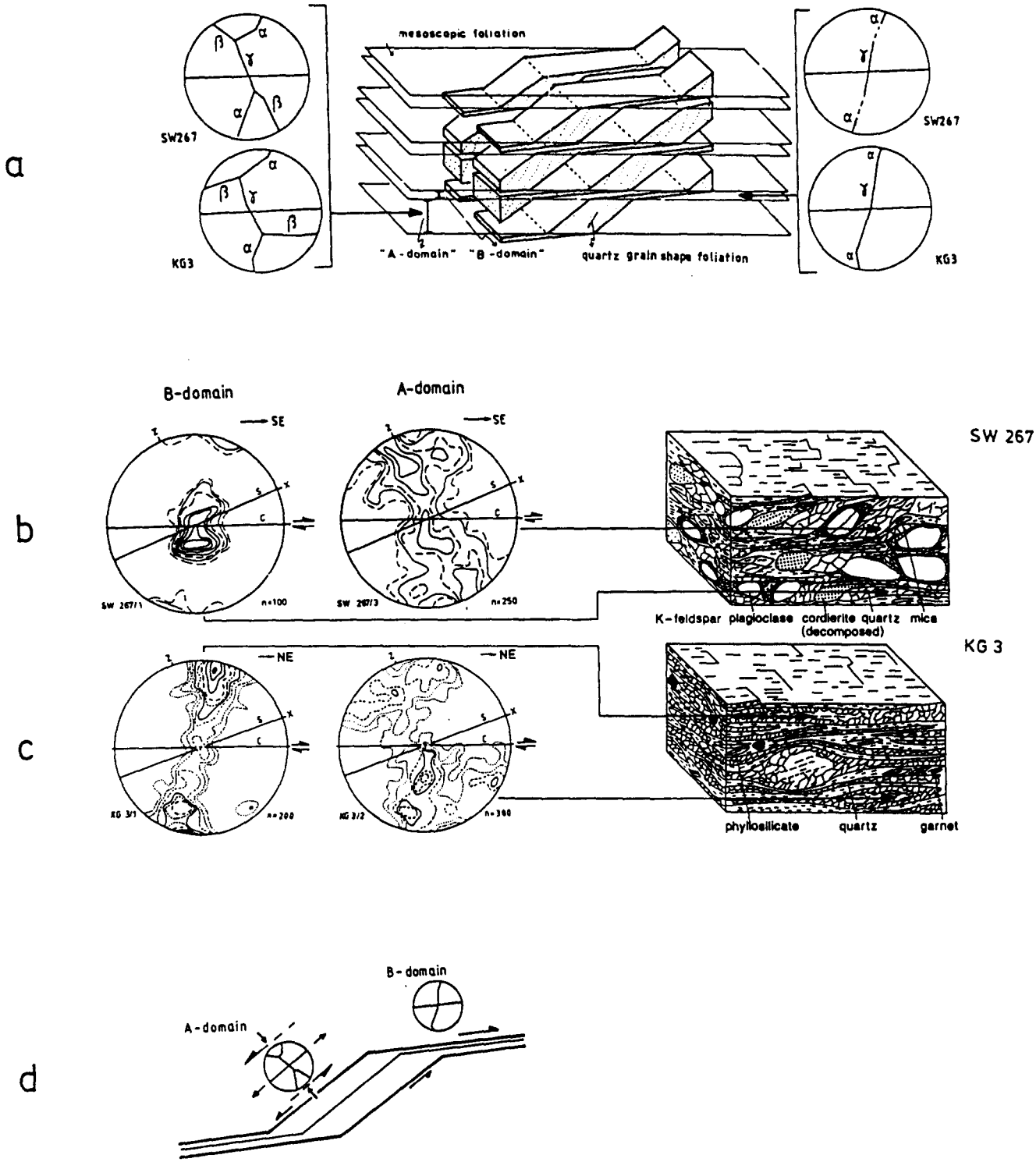

Fig. 1. Relationships among mesoscopic and microscopic structures. (a) Illustrative sketch of the planar and linear elements of both specimens. A mesoscopic foliation is defined by compositional layering. Two domains (A and B), which differ in magnitude of strain, deformation mechanism and other parameters of the deformation, extend parallel to the mesoscopic foliation. The domains are characterized by internal planar fabrics that are defined by shape preferred orientation of the mineral aggregates ('A-foliations' and 'B-foliations'). The contact between A- and B-domains is a plane of discontinuity (see text). 'Fabric skeletons' (Lister & Williams 1979) of [c]-axis diagrams are shown. In the A-domains in both specimens, quartz [c]-axis type I crossed-girdles exhibit a near rhombohedral internal symmetry (left), which is defined by two crossed-girdles α and β that are symmetric to the connecting girdle γ and that contain an equal pole density. The pole figure is inclined against the sense of shear with respect to the mesoscopic foliation. In the B-domain (right) the skeleton is a straight single-girdle that is slightly inclined towards the sense of overall shear (specimen KG3), or a strong point maximum, slightly elongate normal to the X axis, near the inferred finite Y axis (specimen SW267). (b) & (c) Microstructures of (b) specimen SW267 and (c) specimen KG3. Secondary cleavages have been omitted. Newly formed quartz grains are not true to scale. Representative quartz [c]-axis textures of the A- and B-domains are shown. C is the trace of the mesoscopic foliation and S the trace of the A-foliation. Contours: KG3, A-domain (KG3/2): 0.5, 1, 2, 3, 4 and 6% per 1% area; KG3, B-domain (KG3/1): 0.5, 1, 2, 3, 4, 6, 8, 10 and 12% per 1% area; SW267, A-domain (SW267/2): 0.5, 1, 2, 3 and 4% per 1% area; SW267, B-domain (SW267/1): 1, 2, 4, 6, 8, 12 and 16% per 1% area. (d) The alignment of the [c]-axes in two crossed-girdles (A-domain) and one single-girdle (B-domain) suggests spatial partitioning of the strain path (see text).

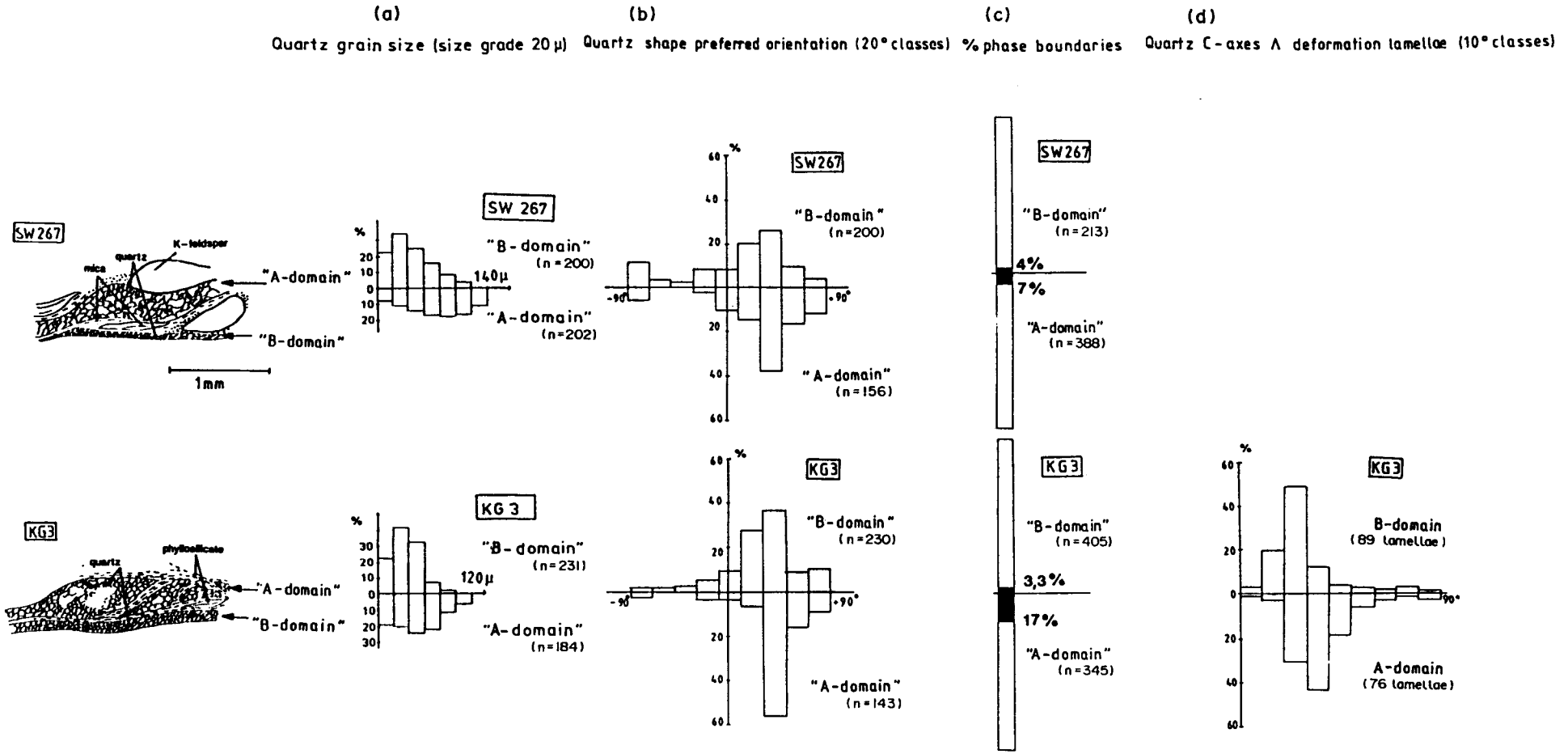

Fig. 2. Microstructures of the A- and B-domains of specimens SW267 and KG3 (*XY* sections). (a) Frequency distribution of grain sizes of recrystallized quartz. (b) Shape preferred orientation of newly formed quartz grains. The diagrams show the frequency distribution of angle between the long axes of grains and the trace of the mesoscopic foliation. (c) Frequency of phase boundaries (mostly between quartz and phyllosilicates) vs grain (quartz against quartz) boundaries. The measurements were carried out on traverses normal to the mesoscopic foliation. The A-domain of specimen KG3 is characterized by a relatively high proportion of phase boundaries. (d) Frequency distribution of angle between the pole to the deformation lamellae and the [*c*]-axis of the corresponding grain. (Lamellar features were only observed in specimen KG3.)

mately normal to the measured A-foliation (specimen SW267), or slightly inclined with respect to this foliation, in a sense opposite to the overall sense of shear (specimen KG3). The quartz [c]-axes show a generally higher degree of preferred orientation in the B-domains of both specimens than they do in the A-domains. In specimen KG3 the pole figure is a single-girdle at high angle to the lineation and inclined in the overall sense of shear with respect to the mesoscopic foliation. In specimen SW267 the pole figure is a point maximum near the inferred finite *Y* axis; there are only a few points at high angle to the lineation.

DISCUSSION

Quartz [c]*-axis fabric skeletons as indicators for local variations in the orientation of the 'easy glide direction'*

Variations in [c]-axis fabric skeletons and in degree of [c]-axis preferred orientation (Figs. 1a–d) could reflect variations in the operative glide systems and/or in orientation of the easy glide direction. They could also reflect varying influences of the earlier deformation history. In the following discussion it is inferred that the [c]-axis patterns in the A- and B-domains of both specimens developed by glide along the crystallographic ⟨a⟩ direction. The orientation of the easy glide system, however, cannot be deduced exclusively from the [c]-axis fabrics. It was not possible to measure the corresponding ⟨a⟩-axis distributions by X-ray diffraction methods—the domain in which measurements were made with the U-stage are only a few millimeters in dimension, and on a larger scale than this both specimens are inhomogeneous in fabric and mineral composition. ⟨a⟩-axis orientations corresponding to [c]-axis patterns of the kind described in this paper were presented by Schmid & Casey (1986) (shown in Fig. 3). Type I [c]-axis crossed-girdles, characterized by an internal symmetry and by equal density of poles within both partial girdles, are observed in the A-domains. They resemble the [c]-axis patterns of specimens PT463 and RL8215 (Fig. 3). The corresponding ⟨a⟩-axes are concentrated in two maxima within the *XY* plane, perpendicular to the [c]-axis partial girdles. Schmid & Casey (1986) suggested that this orientation reflects conjugate glide along ⟨a⟩ on the basal, rhomb and prism planes. It is the most appropriate orientation for the accommodation of two-dimensional strain within the *XY* plane in coaxial (plane strain) regimes.

A [c]-axis single girdle, characterized by a strong maximum at high angle to the *XY* plane, is observed in the B-domains of specimen KG3. It resembles the [c]-axis pattern of specimen C156 (Fig. 3), in which the ⟨a⟩ axes are aligned along a single maximum within the *XY* plane, normal to the [c]-axis girdle. Schmid & Casey (1986) suggested that this orientation reflects glide along ⟨a⟩ on the basal, rhomb and prism planes in one direction only. It is the most appropriate orientation for the accommodation of two-dimensional strain within the *XY* plane in non-coaxial (simple shear) regimes. A strong [c]-axis maximum within the [c]-axis girdle at high angle to the inferred finite *XY* plane suggests a predominance of ⟨a⟩ glide on the basal planes of specimen KG3.

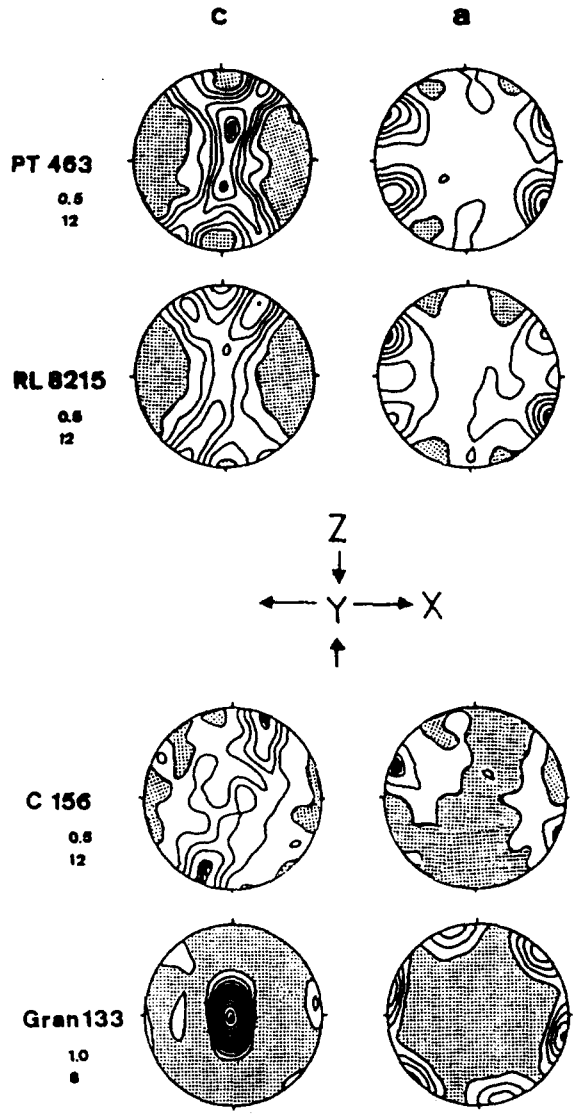

Fig. 3. [c]-axis patterns and corresponding ⟨a⟩-axis orientations presented by Schmid & Casey (1986). The [c]-axis patterns are similar to those observed in this paper. Specimens PT463 and RL8215: [c]-axis type I crossed-girdle—the ⟨a⟩ axes are aligned within the *XZ* plane perpendicular to the [c]-axis girdles. Specimen C-156: [c]-axis single girdle containing a maximum at a high angle to the *X* axis—the ⟨a⟩-axes are aligned along one single maximum normal to the [c]-axis girdle. Specimen Gran133: [c]-axis point maximum parallel to the *Y* axis—the ⟨a⟩-axes show three maxima within the *XZ* plane that reflect a 'single crystal position'.

The [c]-axis point maximum near the inferred finite *Y* axis observed in specimen SW267 resembles the [c]-axis pattern of specimen Gran 133 (Fig. 3), in which the corresponding ⟨a⟩-axis distribution shows three maxima within the *XY* plane normal to the [c]-axis maximum, reflecting a 'single crystal position'. Different positions of the ⟨a⟩-axis maxima with respect to the *X* and *Z* axes were discussed by Schmid *et al.* (1981). In coaxial regimes the ⟨a⟩-axis maxima could be distributed symmetrically about the *X* axis (with one maximum parallel to the foliation normal, *Z*), and in non-coaxial regimes they could be inclined with respect to the *X* and *Z* axes

(see specimen Gran 133 in Fig. 3). In both cases identical [c]-axis patterns develop.

In the following section the kinematic significance of the observed [c]-axis variations is discussed. There are two basic questions.

(1) Do the variations in quartz [c]-axis orientations reflect differences in the strain path between the A- and B-domains? Do they also reflect differences in other parameters of the deformation?

(2) Do the variations in quartz [c]-axis orientations reflect different stages of the deformation history?

'Steady state' orientation of glide systems

A model which may provide an explanation for lattice preferred orientation of minerals with a limited number of glide systems, as is probably the case in naturally deformed quartz (Schmid & Casey 1986), was presented by Etchecopar (1977) and Etchecopar & Vasseur (1987). According to that model, at any instant of the deformation the state of stress within the aggregate is supposed to be homogeneous; a grain is considered to be perfectly fluid along one single glide system ('easy glide system') but undeformable in any other direction. The magnitude of strain accommodated by an individual grain depends mainly on the resolved shear stress acting upon the easy glide system. A polycrystalline aggregate deforms heterogeneously. Grains with their easy glide system aligned in a direction of high resolved shear stress are allowed to accommodate higher strains than grains not so aligned. Preferred orientation is caused by rigid body rotation (Nicholas & Poirier 1976, Etchecopar 1977) of the grains to achieve a best-fit.

In coaxial regimes, after some increments of strain the glide systems have the tendency to rotate towards a direction of lower resolved shear stress and cease to operate (see below). This mechanism of strengthening has to be balanced by the operation of a weakening mechanism to maintain continuous slip at constant strain rate, $\dot{\varepsilon}_c$. Thus $\dot{\varepsilon}_c = \dot{\omega}/\dot{h}$ (where $\dot{\omega}$ = weakening rate, $\dot{h}$ = hardening rate).

Reorientation of the easy glide systems towards a direction of high resolved shear stress is probably controlled by dynamic recovery and recrystallization. After the easy glide systems have rotated into a direction of low resolved shear stress, deviatoric stress within the crystal rises and the density of dislocations becomes higher on glide systems that are more difficult to activate (increasing the level of stored strain energy). Dynamic recovery driven by rearrangement of these dislocations into a lower energy configuration causes bulk lattice rotation ('rotation recrystallization') in KG3. A constant orientation of active glide systems develops (see Means 1981), in which the weakening (or accommodation) rate and the hardening rate (rotation rate of the glide system towards a direction of low resolved shear stress) are in equilibrium. Alternatively, after the easy glide system has rotated into an orientation of lower resolved shear stress, slip may be activated on several other, stronger glide systems that are more favorably orientated. Grains so affected are also assumed to have higher stored strain energy levels (cf. Jessel 1988a) and will be consumed by adjacent grains that are more favorably oriented for slip on the easy glide system (Jessel 1986). In the following it is assumed that the observed crystallographic preferred orientations of quartz in the samples analysed in this paper represent steady state orientations of the easy glide systems.

Kinematic significance of the observed spatial variations in [c]*-axis orientations*

Two stable positions of the easy glide system may be generated in coaxial and non-coaxial regimes. This is demonstrated in Fig. 4. In the left column of the large diagrams, the direction and velocity of rotation of glide planes during deformation are shown by the direction and length of the arrows (according to the simulations of Etchecopar 1977). Three classes of glide systems, indicated by numbers in the diagrams, have been distinguished on the basis of their initial orientation. In the right column of the large diagrams the resolved shear stress acting on any plane is shown as a function of the instantaneous orientation of the glide plane. The reference frame for the angles plotted in the diagrams is shown in the small diagrams on the right.

(1) In coaxial regimes (Fig. 4a) glide systems of any initial orientation tend to rotate towards the X axis of finite strain. Glide is strengthened along systems initially oriented at a low angle to X (zone 3) at any instant of the deformation history because the glide systems tend to rotate towards an orientation of lower resolved shear stress. Glide is weakened along systems initially oriented at between 40° and 85° to X (zone 1) in the initial stages of the deformation history because there is an increase of resolved shear stress acting upon these planes as they rotate. After some increments of strain, when they have rotated to a low angle to X, glide on these systems is also strengthened. No glide occurs at the first instant of the deformation on glide systems initially oriented at about 90° to the X axis of finite strain (zone 2). After some increments of strain the glide systems rotate through zone 1, where glide is rapidly weakened, into zone 3, where glide is strengthened. The quartz aggregate can only accommodate higher strain by dislocation creep if the rotation of the glide systems towards X (producing strengthening of the crystallographic preferred orientation) is balanced by a process which weakens crystallographic preferred orientation (e.g. recovery and recrystallization). The result is that two stable positions of the easy glide system, disposed symmetrically about the X axis, are generated at a low angle to X (normal to the α- and β-girdles). Alignment of a glide system along one or other stable position is only a function of its initial orientation.

(2) In non-coaxial regimes (Fig. 4b) the majority of the glide systems tend to rotate in the sense of the overall rotational strain. Glide is weakened along systems initially oriented between −30° and +50° to the bulk shear plane (SP) (zone 1). Such systems tend to

rotate towards SP, which is a position of maximum resolved shear stress. Glide is strengthened along systems initially oriented between +50° and +95° to SP (zone 3). Glide is weakened in the early stages and stengthened in the later stages of the deformation history on systems initially oriented between −30° and −85° (zone 2) to SP. Glide systems initially oriented in zones 2 and 3 tend to rotate towards a position of zero resolved shear stress at about 45° to SP. The quartz aggregate can only accommodate higher strain by dislocation creep along these systems, if (1) the effect of rotation is counterbalanced before the glide systems reach the position of zero resolved shear stress; or (2) if they are able to pass through the position of zero resolved shear stress and rotate further towards SP.

Two stable positions of the easy glide system are generated. The first ('low-angle position' approximately normal to the α-girdle) is oriented close to SP and the second ('high-angle position', approximately normal to the β-girdle) is oriented at about +50° to SP. Alignment of a glide system in one or other stable position is a function of its initial orientation, of parameters of deformation (strain and strain rate) and of rate of recovery and recrystallization (during which the volume fraction

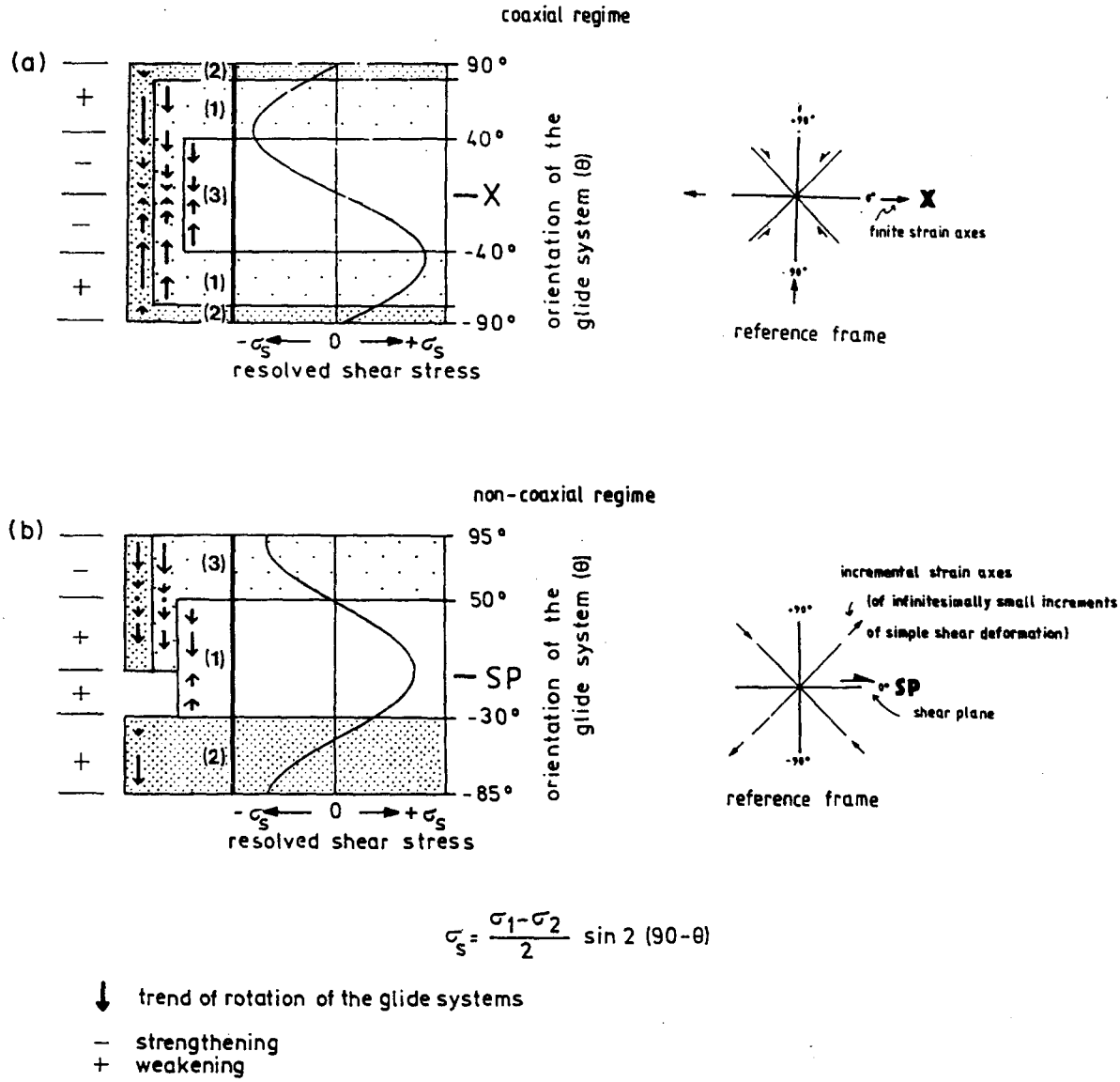

Fig. 4. Possible stable positions of the easy glide systems in two conjugate directions in (a) coaxial and (b) non-coaxial (clockwise) regimes. In the left column of the main diagrams the directions and velocities of rotation of the glide planes during deformation are shown by the directions and lengths of the arrows (according to the simulations of Etchecopar 1977). Three classes of glide systems, indicated by numbers, have been distinguished on the basis of their initial orientation. In the right column of the main diagrams the resolved shear stress acting on any plane is shown as a function of its instantaneous orientation. The reference frame for the angles plotted in the main diagrams (left) are shown on the small diagrams (right). (a) Coaxial regimes. During deformation individual glide systems generally have the tendency to rotate towards lower angles to X. After some increments of strain, when all glide systems have been rotated towards an angle <45° to X, the strength increases on all glide systems with increasing strain. Two stable orientations, disposed symmetrically about X, are generated. (b) Non-coaxial regimes. During deformation individual glide systems initially oriented in zone 1 have the tendency to rotate towards the bulk shear plane; glide systems initially oriented in zones 2 and 3 tend to rotate towards a position of zero resolved shear stress at about 45° to the SP. Two stable positions of the easy glide system—oriented at about +50° (normal to the β-girdle) and subparallel to the bulk shear plane (approximately normal to the α-girdle) may be generated (see text for discussion).

of grains whose easy glide system has been rotated into a low resolved shear stress orientation decreases in favor of grains whose easy glide systems are in positions of high resolved shear stress). After some strain increments, most of the glide systems initially oriented in zones 2 and 3 will be aligned in the high-angle position and glide along these systems will be strengthened. At low recovery/recrystallization rates, higher strain is accommodated at constant strain rate only by glide on systems that are in the low-angle stable position. At high recovery/recrystallization rates, higher strain may be accommodated at a constant (low) strain rate by glide on systems that are aligned in both low- and high-angle stable positions: towards higher strain rates, the easy glide systems aligned in the high-angle position, normal to the β-girdle increasingly become able to pass through the position of zero resolved shear stress and the number of glide systems aligned that position decreases in favor of the number of glide systems aligned in the low-angle position (cf. Bouchez & Duval 1982).

The observed [c]-axis variations can be interpreted in two different ways.

(1) Quartz [c]-axis variations are due to partitioning of an overall rotational flow path between domains that underwent spinning coaxial (A-domain) and domains that underwent non-spinning non-coaxial deformation (B-domain) (Fig. 5). The terms coaxial/non-coaxial are related to the angular velocity of the finite strain axes with respect to the instantaneous stretching axes (or the principal directions of incremental strain in Fig. 4b) and the terms spinning/non-spinning are related to the angular velocity of the instantaneous stretching axes with respect to an external reference frame (Means *et al.* 1980). Type I crossed-girdles, which are characterized by an internal rhombohedral symmetry, are symmetric to the principal directions of a local coaxial finite strain that is close to plane strain (A-domain; cf. Lister & Williams 1979). The pole density in the α- and β-girdles depends on the component of non-coaxial flow. Single-girdle fabrics are suggested to be normal to the direction of a local simple shear strain (B-domain).

(2) Quartz [c]-axis variations are due to partitioning of an overall rotational flow path between domains that underwent spinning non-coaxial deformation (A-domain), in which the glide systems have the tendency to rotate towards orientations of lower resolved shear stress, and domains that underwent non-spinning non-coaxial deformation (B-domain, Fig. 5), in which the glide systems do not rotate towards lower resolved shear stress orientations. Consequently, strain path partitioning is associated with difference in parameters of deformation between the two domains, i.e. differences in strain and strain rate.

At a low recovery/recrystallization rate, after some strain increments, deformation will cease in the A-domains. At a high recovery/recrystallization rate, at a constant (low) strain rate, deformation may continue in the A-domains; an increasing strain rate (from the A- to the B-domains) will result in a higher density of poles on the α-girdle and a lower density of poles on the β-girdle (Fig. 1a). In the case of interpretation (2) 'type I' crossed-girdles reflect neither the direction of finite strain nor the sense of shear.

Temporal variations of quartz [c]*-axis orientations*

The deformational behavior of the bulk quartz volume may be compared to that of a two phase aggregate, which is composed of a strong and a weak phase, as described by Jordan (1987). The A-domains which accumulated only moderate strain represent the stronger phase. The B-domains which accumulated higher strain reflect the weaker phase. They suffered a higher degree of strain weakening than the A-domains. An overall shear strength that is lower in the B-domains than in the A-domains is inferred from the [c]-axis textures.

(1) In the case of overall non-coaxial strain (see point

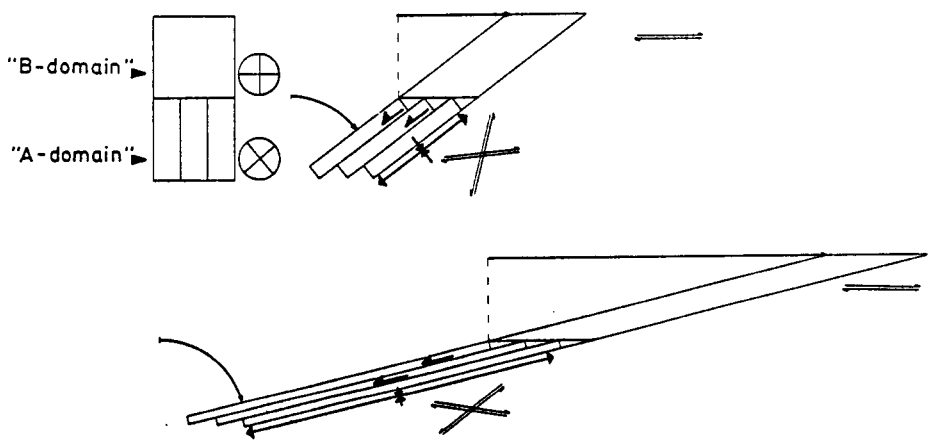

Fig. 5. Strain path partitioning between aggregates that are larger than the measured cell. An overall rotational flow path is partitioned into two domains. The upper part of the block (corresponding to the B-domains in Fig. 1) undergoes homogeneous simple shear (non-spinning, non-coaxial deformation). The lower part of the block (corresponding to the A-domains in Fig. 1) undergoes (1) stretching and rigid body rotation (spinning coaxial deformation), (2) antithetic slip and rigid body rotation (spinning non-coaxial deformation), or (3) strain path partitioning between (1) and (2) (as shown in the figure).

2 in the previous section) the overall shear strength of the quartz aggregate is a function of the volume ratio of grains oriented with their easy glide system in high-angle and low-angle stable positions. If the volume of the grains oriented in the high-angle position (that is those grains that rotate towards a locked position) decreases, as is the case in the B-domains, the overall shear strength of the quartz aggregate is lowered.

(2) A high degree of preferred orientation of the weakest glide system along the shear plane also results in a reduction in overall shear strength. In the B-domains a single maximum within the [c]-axis girdle suggests that glide (possibly along ⟨a⟩) on one plane, presumably the weakest, has increased and glide along stronger systems has decreased.

After a critical volume of B-domains has been formed as a result of increasing fabric weakening, the shear strength of the bulk quartz volume approximates that of the B-domains: residual A-domains behave like rigid objects in a ductile matrix, remain unaffected by further internal deformation, and preserve their older [c]-axis texture. In all domains, however, the pole figures are symmetric with respect to a plane defined by the mesoscopic lineation and the normal to the mesoscopic foliation. The fabrics of the A- and B-domains are considered to have developed at different stages of the same deformation process.

CONCLUSIONS

The final preserved quartz [c]-axis textures of S–C mylonites are inferred to have developed by slip along the crystallographic ⟨a⟩ direction. They are considered to reflect steady-state orientations of the easy glide systems (⟨a⟩ slip) during different stages of the deformation history. The [c]-axis orientations of moderately deformed domains (A-domains) show 'type I' crossed-girdles, which are inclined in a sense opposite to the overall sense of shear. They are characterized by a near rhombohedral internal symmetry. The [c]-axis orientations of more strongly deformed domains (B-domains) show single-girdles, which are slightly inclined towards the sense of shear.

Differences in quartz [c]-axis textures between the A- and B-domains can be generated in different ways.

(1) Quartz [c]-axis variations may reflect spatial partitioning of flow path between domains that underwent spinning coaxial flow (A-domains), and those that underwent non-spinning, non-coaxial (B-domains) flow. Type I crossed-girdle fabrics are considered to be symmetric with respect to the axes of a local finite coaxial strain. Only single-girdle fabrics characterize a local non-coaxial strain. Their asymmetry indicates the sense of shear.

(2) Quartz [c]-axis variations may reflect spatial partitioning in flow between domains that underwent spinning, non-coaxial flow (A-domains) and those that underwent non-spinning, non-coaxial (B-domains) flow. Strain path partitioning is associated with partitioning in parameters of the deformation (such as strain, strain rate). The change from a crossed to a single [c]-axis girdle is also suggested to be an effect of recovery and recrystallization. The orientation of crossed-girdles reflects neither the orientation of a local finite strain nor the sense of shear. The sense of shear is indicated only by single girdle fabrics.

Shear-sense determinations based on asymmetric crossed-girdles should be carried out carefully. Crossed-girdles that are indicative of the sense of shear should be characterized by: (1) fabric skeletons should exhibit an internal asymmetry; (2) the pole density in the α-girdle should be higher than in the β-girdle; (3) the external asymmetry of the pole figure with respect to local strain axes (defined by the '*S*-plane') should be consistent with (1) and (2). In any case single-girdles provide much more reliable shear-sense data than crossed-girdles.

The transition in texture from the A- to the B-domains is associated with fabric weakening. The quartz textures are considered to have developed at different stages during the same deformation process. The skeletons of [c]-axis pole figures in the A- and B-domains show similar patterns irrespective of whether glide along ⟨a⟩ was predominantly on the prism planes or on the basal planes.

Acknowledgements—I wish to thank P. Hudleston, an anonymous reviewer and in particular R. D. Law for constructive criticisms, which substantially improved the scientific aspect of the manuscript. B. Stöckhert and A. Willner made helpful suggestions about an earlier version of this work. Investigations in the Schwarzwald were financially supported by the Deutsche Forschungsgemeinschaft.

REFERENCES

Ardell, A. J., Christie, J. M. & McCormick, J. W. 1974. Dislocation images and determination of the burgers vectors. *Phil. Mag.* **29**, 1399–1411.

Baëta, R. D. & Ashbee, K. H. G. 1969a. Slip systems in quartz: I experiments. *Am. Miner.* **54**, 1551–1573.

Baëta, R. D. & Ashbee, K. H. G. 1969b. Slip systems in quartz: II experiments. *Am. Miner.* **54**, 1574–1582.

Behrmann, J. H. & Platt, J. P. 1982. Sense of emplacement from quartz *c*-axes; an example from the Betic Cordilleras (Spain). *Earth Planet. Sci. Lett.* **58**, 208–215.

Bouchez, J. L. 1978. Preferred orientation of ⟨a⟩ axes in some tectonites: kinematic inferences. *Tectonophysics* **49**, 725–750.

Bouchez, J. L. & Duval, P. (1982). The fabric of polycrystalline ice deformed in simple shear: experiments in torsion, natural deformation and geometrical interpretation. *Text. Microstruct.* **5**, 171–190.

Burg, J.-P. & Laurent, P. 1978. Strain analysis of a shear zone in a granodiorite. *Tectonophysics* **47**, 15–42.

Burg, J.-P., Wilson, C. J. C. & Mitchell, J. C. 1986. Dynamic recrystallization and fabric development during simple shear deformation of ice. *J. Struct. Geol.* **8**, 857–870.

Etchecopar, A. 1977. A plane kinematic model of progressive deformation in a polycrystalline aggregate. *Tectonophysics* **39**, 121–139.

Etchecopar, A. & Vasseur, G. 1987. A 3-D kinematic model for fabric development in polycrystalline aggregates: comparison with experimental and natural examples. *J. Struct. Geol.* **9**, 705–718.

Eisbacher, G. H. 1970. Deformation mechanics of mylonite rocks and fractured granites in Cobequid Mountains, Nova Scotia, Canada. *Bull. Soc. geol. It.* **81**, 2009–2020.

Garcia Celma, A. 1982. Domainal and fabric heterogeneities in the Cap de Creus quartz mylonites. *J. Struct. Geol.* **4**, 443–455.

Hobbs, B. E., McClaren, A. C. & Paterson M. S. 1972. Plasticity of

single crystals of synthetic quartz. In: *Plasticity of Single Crystals of Synthetic Quartz* (edited by Heard, H. C., Borg, I. Y., Carter, N. L. & Raleigh, C. B.). *Am. Geophys. Un. Geophys. Monogr.* **16**, 29–53.

Hobbs, B. E., Means, W. D. & Williams, P. F. 1976. *An Outline of Structural Geology*. Wiley, New York.

Jessel, M. W. 1986. Grain boundary migration and fabric development in experimentally deformed octachloropropane. *J. Struct. Geol.* **8**, 527–542.

Jessel, M. W. 1988a. Simulation of fabric development in recrystallizing aggregates—I. Description of the model. *J. Struct. Geol.* **10**, 771–778.

Jessel, M. W. 1988b. Simulation of fabric development in recrystallizing aggregates—II. Example model runs. *J. Struct. Geol.* **10**, 779–793.

Jordan, P. G. 1987. The deformational behaviour of bimineralic limestone–halite aggregates. *Tectonophysics* **135**, 185–197.

Kirby, S. H. 1977. The effects of the alpha–beta phase transformation of the creep properties of hydrolytically weakened synthetic quartz. *Geophys. Res. Lett.* **4**, 97–100.

Krohe, A. 1987 Kinematics of Cretaceous nappe tectonics in the Austroalpine basement of the Koralpe region (eastern Austria). *Tectonophysics* **136**, 171–196.

Krohe, A. & Eisbacher, G. H. 1988. Oblique crustal detachment in the Variscan Schwarzwald, southwestern Germany. *Geol. Rdsch.* **77**, 25–43.

Law, R. D., Casey, M. & Knipe, R. J. 1986. Kinematics and tectonic significance of microstructures and crystallographic fabrics within quartz mylonites from the Assynt and Eriboll regions of the Moine thrust zone, N. W. Scotland. *Trans. R. Soc. Edinb., Earth Sci.* **77**, 99–126.

Law, R. D., Knipe, R. J. & Dayan, H. 1984. Strain path partitioning within thrust sheets: microstructural and petrofabric evidence from the Moine Thurst zone at Loch Eriboll, northwest Scotland. *J. Struct. Geol.* **6**, 477–497.

Law, R. D. 1986. Relationships between strain and quartz crystallographic fabrics in the Roche Maurice quatzites of Plougastel, western Brittany. *J. Struct. Geol.* **8**, 493–515.

Law, R. D. 1987. Heterogeneous deformation and quartz crystallographic fabric transitions: natural examples from the Moine Thrust zone at the Stack of Glencoul, northern Assynt. *J. Struct. Geol.* **9**, 819–833.

Linker, M. E., Kirby, S. H., Ord, A. & Christie, J. M. 1984. Effects of compression direction of the plasticity and rheology of hydrolytically weakened synthetic quartz crystals at atmospheric pressures. *J. geophys. Res.* **89**, 4241–4255.

Lister, G. S. 1977. Discussion: crossed-girdle *c*-axis fabrics in quartzites plastically deformed by plane strain and progressive simple shear. *Tectonophysics* **39**, 51–53.

Lister, G. S. & Snoke, A. W. 1984. S–C Mylonites. *J. Struct, Geol.* **6**, 617–638.

Lister, G. S. & Williams, P. F. 1979. Fabric development in shear zones: Theoretical controls and observed phenomena. *J. Struct. Geol.* **4**, 283–297.

Mancktelow, N. S. 1985. The Simplon Line: A major displacement zone in the Western Lepontine Alps. *Eclog. geol. Helv.* **78**, 73–96.

Mancktelow, N. S. 1987. Quartz textures from the Simplon fault zone. SW Switzerland and N Italy. *Tectonophysics* **135**, 133–153.

Means, W. D. 1981. The concept of steady state foliation. *Tectonophysics* **78**, 179–199.

Means, W. D., Hobbs, B. E., Lister, G. S. & Williams, P. W. 1980. Vorticity and non-coaxiality in progressive deformation. *J. Struct. Geol.* **2**, 371–378.

Morrison–Smith, D. J., Paterson, M. S. & Hobbs, B. E. 1976. An electron microscope study of plastic deformation in single crystals of synthetic quartz. *Tectonophysics* **33**, 43–79.

Nicolas A. & Poirier, J. P. 1976. *Crystalline Plasticity and Solid State Flow in Metamorphic Rocks*. Wiley, New York.

Passchier, C. W. 1983. The reliability of asymmetric *c*-axis fabrics of quartz to determine sense of vorticity. *Tectonophysics* **99**, 9–18.

Platt, J. P. & Vissers, R. L. M. 1980. Extensional structures in anisotropic rocks. *J. Struct. Geol.* **2**, 397–410.

Platt, J. P. & Behrmann, J. H. 1986. Structures and fabrics in a crustal-scale shear zone, Betic Cordillera, SE Spain. *J. Struct. Geol.* **8**, 15–33.

Price, G. P. 1985. Preferred orientation in quartzites. In: *Preferred Orientation in Deformed Metals and Rocks: An Introduction to Modern Texture Analysis* (edited by Wenk, H.-R.). Academic Press, London, 385–405.

Schmid, S. M. & Casey, M. 1986. Complete fabric analysis of some commonly observed quartz c-axis patterns: In: *Mineral and Rock Deformation: Laboratory Studies* (edited by Hobbs, B. E. & Heard, H. C.). *Am. Geophys. Un. Geophys. Monogr.* **36**, 263–286.

Schmid, S. M. Casey, M. & Starkey, J. 1981. An illustration of the advantages of a complete texture analysis described by the orientation distribution function (ODF) using quartz pole figure data. *Tectonophysics* **78**, 101–117.

Simpson, C. 1980. Oblique girdle orientation patterns of quartz *c*-axes from a shear zone in the basement core of the Maggia nappe, Ticino, Switzerland. *J. Struct. Geol.* **2**, 243–247.

Simpson, C & Schmid, S. M. 1983. An evaluation of criteria to deduce the sense of movement in sheared rocks. *Bull. Geol. Soc. Am.* **94**, 1281–1288.

Taylor, G. I. 1938. Plastic strain in metals. *J. Inst. Metals* **62**, 307–324.

Takeshita, T. & Wenk, H.-R. 1988. Plastic anisotropy and geometrical hardening in quartzites. *Tectonophysics* **149**, 345–361.

Twiss, R. J. 1976. Some planar deformation features, slip systems, and submicroscopic structures in synthetic quartz. *J. Geol.* **84**, 701–704.

Van Roermund, H., Lister, G. S. & Williams, P. F. 1979. Progressive development of quartz fabrics in a shear zone from Monte Mucrona, Sezia-Lanzo zone, Italian Alps. *J. Struct. Geol.* **1**, 43–52.

Vauchez, A. 1987. The development of discrete shear zones in a granite: stress, strain and changes in deformation mechanisms. *Tectonophysics* **133**, 137–156.